Detection of Saccades and Postsaccadic Oscillations in the Presence of Smooth Pursuit

Linnéa Larsson*, Marcus Nyström, and Martin Stridh

***Abstract*—A novel algorithm for detection of saccades and postsaccadic oscillations in the presence of smooth pursuit movements is proposed. The method combines saccade detection in the acceleration domain with specialized on- and offset criteria for saccades and postsaccadic oscillations. The performance of the algorithm is evaluated by comparing the detection results to those of an existing velocity-based adaptive algorithm and a manually annotated database. The results show that there is a good agreement between the events detected by the proposed algorithm and those in the annotated database with Cohen's kappa around 0.8 for both a development and a test database. In conclusion, the proposed algorithm accurately detects saccades and postsaccadic oscillations as well as intervals of disturbances.**

***Index Terms*—Eye-tracking, signal processing, smooth pursuit.**

I. Introduction

MEASUREMENT of eye movements is important for basic research in visual attention, perception, and cognition, as well as for clinical applications investigating the functionality of the brain or to diagnose physiological disorders, such as Alzheimer's [1], HIV-1 infected patients with eye movement dysfunction [2], and schizophrenia [3]. The interest in eye-tracking is also increasing in applied fields with strong commercial interests, e.g., web page navigation, online shopping, and interaction with computers. An important new development in the field is that eye movement studies are starting to use more realistic dynamic scenes as stimuli, e.g., short videos, compared to earlier when mainly static images were used. Since the tools for analyzing eye movement signals are mainly developed for static images, the use of dynamic scenes requires a new set of algorithms for the segmentation of recorded signals into eye movement events. In order to be able to draw correct conclusions about the underlying processes in the brain or to be able to control a computer, reliable algorithms for the detection and classification of eye movements are crucial.

Manuscript received June 29, 2012; revised September 20, 2012, February 15, 2013, and April 8, 2013; accepted April 14, 2013. Date of publication April 18, 2013; date of current version August 16, 2013. This work was supported by the Strategic Research Project eSSENCE, founded by the Swedish Research Council. *Asterisk indicates corresponding author.*

*L. Larsson is with the Department of Electrical and Information Technology, Lund University, Lund 221 00, Sweden (e-mail: linnea.larsson@eit.lth.se).

M. Nyström is with the Lund Humanities Laboratory, Lund University, Lund 223 62, Sweden (e-mail: marcus.nystrom@humlab.lu.se).

M. Stridh is with the Department of Electrical and Information Technology, Lund University, Lund 221 00, Sweden (e-mail: martin.stridh@eit.lth.se).

Digital Object Identifier 10.1109/TBME.2013.2258918

When studying eye movements, mainly three movements are identified: the slow period when the eye is more or less still and visual information is taken in is referred to as a $fixation$, which is characterized by low positional dispersion, low velocity, and a duration of about 200–300 ms [4]. When the eye is shifting from one position to another, the movement is referred to as a $saccade$, which is a very rapid movement with typical velocities ranging from 30 to 500 deg/s and durations ranging from 30 to 80 ms [4]. Very little visual information is gathered during saccades [5]. These two eye movements are the most common ones when observing static objects. When the observed objects are moving, e.g., when watching a dynamic scene, other eye movements may occur that are related to the movement in the scene. One such eye movement is the $smooth\ pursuit$, which occurs when the eye has a moving target to follow [5]. The velocity of a smooth pursuit movement depends on the speed of the moving target, but is typically below 30 deg/s [4], even though the velocity can be as high as 100 deg/s [6]. However, for targets with velocities higher than 30 deg/s, the eye movements typically consist of both saccades and smooth pursuit movements. In order for the eye to be able to accurately follow the target, catch-up saccades are required since the pursuit gain falls below one [5].

In addition to these three eye movements, we investigate in this paper the oscillatory behavior that may occur at the end of a saccade. In [7], three different types of movements in connection to the saccade were categorized: dynamic overshoot, which is a fast movement with velocities of 10–100 deg/s, glissadic overshoot which is a slow drifting movement with velocities of 2–20 deg/s, and static overshoot, which is a corrective saccade that starts 200 ms after the primary saccade. In this paper, we are interested in detecting all types of high-velocity transients that may occur at the end of the saccade, e.g., overshoot/undershoot, oscillatory behavior, and immediate changes in direction compared to the preceding saccade. All of these types of movements are referred here to as $postsaccadic\ oscillations$ (PSO).

Algorithms for the detection of eye movements can broadly be divided into two groups: dispersion based and velocity/acceleration-based algorithms. Algorithms based on dispersion are mainly used for signals with a lower sampling frequency ($<$200 Hz), while the velocity/acceleration-based methods are used for signals with a higher sampling frequency ($>$200 Hz) [4]. In recent years, algorithms used for the detection of eye movements have developed from solely using a preset threshold of dispersion or velocity/acceleration [8], toward adaptive algorithms where the thresholds are estimated from the signals [9]–[12]. By using an adaptive threshold, individual differences between participants and trials can be taken into account, and the algorithm becomes less dependent on the

user's ability to correctly set the thresholds. The majority of the adaptive algorithms referred to above are velocity-based and were developed for the detection of eye movements when the stimulus is static and the signals thus do not contain any smooth pursuit movements. However, in signals where the stimulus is dynamic, it is important to also consider the smooth pursuit movements in the detection algorithm, since their presence may otherwise render the detection of the other eye movements difficult. The major problem is that the velocity of a fast smooth pursuit movement overlaps with the velocity range of a slow saccade [11], [13], making it difficult to set a velocity threshold for discrimination between these two types of eye movements [14].

In order to reliably detect saccades in signals where smooth pursuit movements are present, the acceleration signal has been used since the acceleration of saccades is higher than that of smooth pursuit movements [11]. A real-time algorithm where the acceleration signal is employed for the detection of saccades is found in the commercial EyeLink algorithm. In order for a saccade to be detected, a combination of thresholds for changes in position, velocity, and acceleration has to be satisfied [15]. Another real-time algorithm that uses the acceleration signal is the adaptive algorithm proposed in [11]. In order for the algorithm to detect the beginning of the saccade, the acceleration of each sample is compared to a threshold computed from the preceding 200 samples. For the determination of the end of the saccade, a combination of the acceleration threshold and the end of the monotonicity in the position signal for the saccade is employed [11].

Today, there are very few algorithms that include the detection of PSO. A velocity-based adaptive algorithm for the detection of PSO in signals recorded for participants viewing static stimuli was proposed in [9]. As pointed out by the authors, it is important for an algorithm to be consistent to whether the PSO are included in the saccades, in the fixations, or are marked as a separate type of eye movement. This choice is crucial for the calculation of durations of fixations and amplitudes of saccades. While the origin of PSO in pupil-based eye-trackers remains unclear, they have been reported to occur in 48% and 59% of the saccades for participants performing reading and scene perception, respectively [9]. PSOs have been reported in data recorded with Dual Purkinje eye-trackers (DPIs), but were not found in simultaneous recordings with scleral search coils [16]. This suggests that PSO in data recorded by a DPI result from motion of the lens relative to the eyeball rather than motion of the eye in its orbit. To our knowledge, the occurrence and the properties of PSO when viewing a dynamic scene have not been investigated.

In order to objectively evaluate the performance of a detection algorithm for eye movements, the actual movement of the eye needs to be available. Strategies to estimate the actual movement of the eye include to let an expert annotate the signals [4], generate simulated signals [17], or use the stimuli as a reference to the actual eye movement [18]. When evaluating the performance of a detection algorithm for PSO, the only option is to manually annotate the signals, since the occurrence of PSO seems to be involuntary and idiosyncratic [19].

The purpose of this paper is threefold: first, we propose a robust algorithm for the detection of saccades and PSO in signals recorded when viewing static as well as dynamic scenes, where the intrinsic structure is motivated by underlying physiological properties of the saccades and PSO. Second, a mathematical model for describing the properties of PSO is proposed. Third, a framework for the evaluation and comparison of different detection algorithms is proposed, including a graphical user interface (GUI) for presentation of the outputs of detection algorithms and for annotation of signals. The paper is outlined as follows: the proposed algorithm and the evaluation procedure are presented in Section II. A description of the database with eye movement signals is given in Section III. The results are presented in Section IV, and finally, the algorithm and its potential are discussed in Section V.

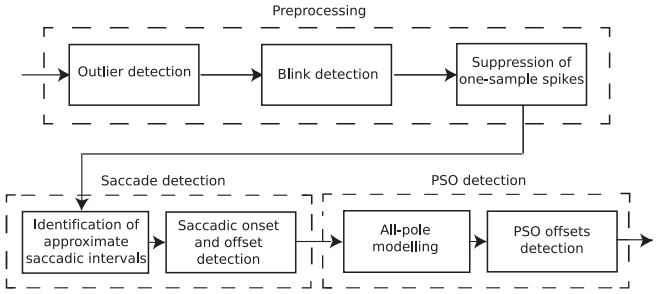

Fig. 1. The overall structure of the algorithm.

II. Methods

The proposed method comprises three different stages: preprocessing, saccade detection, and PSO detection. An overview of the method is shown in Fig. 1. In the first stage, disturbances originating from the recording process are removed. In the second stage, the saccades are detected using criteria reflecting their physiological characteristics, and finally, in the third stage, the detection of PSO is performed.

A. Preprocessing

In the preprocessing stage, three different types of disturbances are excluded from the dataset: screen outliers, blinks, and one-sample spikes. All samples corresponding to positions outside a margin of 1.5° added to the geometry of the stimulus screen are marked as disturbances. During blinks, when the eyelid is closed, the eye-tracker cannot detect the pupil and therefore the eye-tracker used in this study sets the x- and y-coordinates to $(0, 0)$. By detecting these zeros in the position signal, the blinks are detected. However, in the beginning and end of a blink, the eyelid is not completely closed and the pupil can therefore partly be detected. In the position signal, vertical saccade-like movements therefore appear at the start and end of the blink (see Fig. 2(a)). In order to remove as much as possible of the erroneous coordinates caused by the blink, the on- and offsets of the blink are defined as the first local minimum in the y-coordinate, before and after the detected zeros, see the vertical dash-dotted lines in Fig. 2(b). In this paper, the blink duration was limited to 700 ms. Notice that also during other disturbances than blinks when the eye-tracker for some reason cannot detect the pupil, the x- and y-coordinates are set to $(0, 0)$.

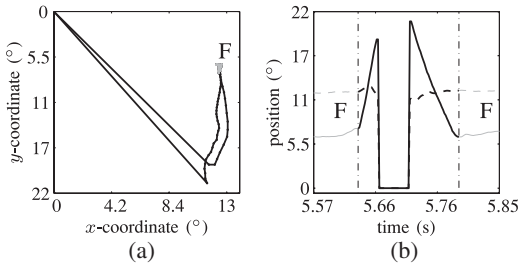

Fig. 2. An example of blink detection. In (a), the vertical saccade-like movement in the y-coordinate in the beginning and in the end of the blink. The black line is showing the blink and the gray line the fixation (F) before and after the blink. In (b), the detection of a blink in the x- (dashed) and y-coordinates (solid) over time. Onset and offset of the blink is marked with dashed-dotted vertical lines, and the black line indicates the blink and the gray line the fixation (F) before and after the blink.

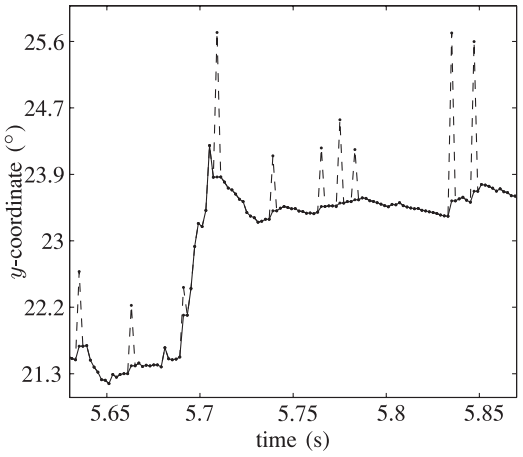

Fig. 3. Example of removal of one-sample spikes, where the dashed line is the unfiltered signal and the solid line is the signal after the one-sample spike suppression.

These disturbances are treated in the same way as blinks and all such samples are marked as disturbances. A common type of disturbance in video-based eye-tracking is that the corneal reflection is not correctly detected in the image of the eye which will result in a rapid positional change of one sample in an unexpected direction and back again. This type of artifact is referred to as a one-sample spike [20]. In order to remove one-sample spikes, a median filter of length 3 can be used [20]. However, in order to remove one-sample spikes but avoid suppressing PSO as well as small variations during fixations, an amplitude and a velocity criteria, of which both need to be satisfied, are used to activate the filter. The amplitude threshold, $a_{\min}$, requires a minimum amplitude of the removed one-sample spike. The value of the parameter $a_{\min}$ is given in Table III, which lists the settings of all intrinsic parameters in the proposed algorithm. The velocity criteria are based on that, since PSO always occurs directly after saccades, the sample-to-sample velocities before PSO are larger than those during PSO. Therefore, the sample-to-sample velocities before a one-sample spike must be lower than those during a one-sample spike. An example of the suppression of one-sample spikes in a signal from the database used in this paper is shown in Fig. 3.

B. Saccade Detection

The first type of eye movement to be detected after the preprocessing stage is the saccade. The detection of saccades is divided into two steps which are shown in the lower left block of Fig. 1.

1) Identification of Approximate Saccadic Intervals: Since saccades, in contrast to both fixations and smooth pursuit movements, are fast eye movements with high acceleration, they are detected in the acceleration domain. The angular velocities, v_x and v_y, are computed by filtering the position signals, $x(n)$ and $y(n)$, using the filter,

$$h(n) = \frac{1}{20}[-1 \quad -1 \quad -1 \quad -1 \quad 0 \quad 1 \quad 1 \quad 1 \quad 1]$$

which is a modified version of the difference and smoothening filter proposed in [10] for signals sampled at 250 Hz. In order for the filter to operate at the same period of time and to give similar effect on signals sampled at 500 Hz, the length of the filter was doubled and the filter coefficients were scaled. The angular accelerations, a_x and a_y, are calculated by applying the same filter to the velocities. In the acceleration signal, *approximate saccadic intervals*, which are segments that include both saccades and possible PSO, are detected. The method used for the delineation of such intervals is based on the method for the detection of microsaccades proposed in [10]. Since the nature of saccades and microsaccades is similar in many aspects, (cf., [21]), the method can be used also for saccade detection. For each of the x- and y-components, the individual acceleration threshold is based on the standard deviations, σ_x and σ_y, of the acceleration distributions. The thresholds are defined as, $\eta_x = \lambda\sigma_x$ and $\eta_y = \lambda\sigma_y$, where λ is a constant that decides how many standard deviations that separates saccades and possible PSO from the rest of the eye movements. Two index vectors indicating the approximate saccadic intervals in the x- and y-components, $I_x(n)$ and $I_y(n)$, are created such that

$$I_x(n) = \begin{cases} 1, & |a_x(n)| > \eta_x \quad \forall n \\ 0, & \text{otherwise} \end{cases}$$

$$I_y(n) = \begin{cases} 1, & |a_y(n)| > \eta_y \quad \forall n \\ 0, & \text{otherwise} \end{cases}$$

where ones indicate saccades or possible PSO and zeros reflect other types of eye movements or disturbances. The index vectors $I_x(n)$ and $I_y(n)$ are merged into one index vector

$$I'(n) = \begin{cases} 1, & I_x(n) = 1 \mid I_y(n) = 1 \\ 0, & \text{otherwise.} \end{cases}$$

Every group of consecutive ones comprises an approximate saccadic interval. Since two saccades cannot appear closer than a certain time, $t_{\min}$, which is the time corresponding to the minimum duration of a fixation, two approximate saccadic intervals that occur closer than $t_{\min}$ are merged and the zeros between are converted to ones. Finally, an approximate saccadic interval must have a duration larger than T ms in order to be valid. The x- and y-components of the acceleration signal for two

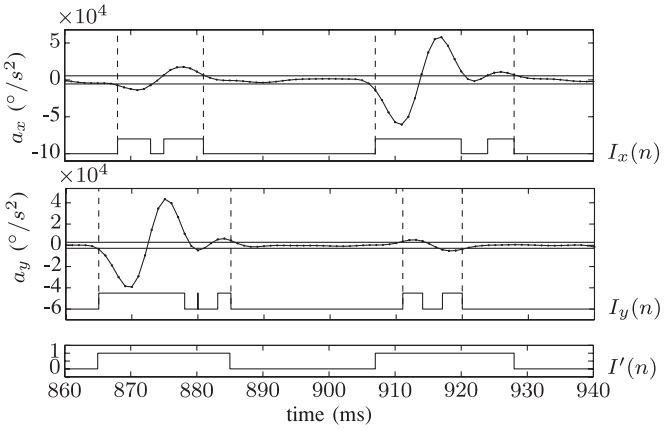

Fig. 4. Example of two consecutive approximate saccadic intervals for the x- and y-components of the acceleration signal, respectively. Below each component, the index vectors $I_x(n)$ and $I_y(n)$ are shown. The bottom panel shows the index vector, $I'(n)$, for the two final approximate saccadic intervals.

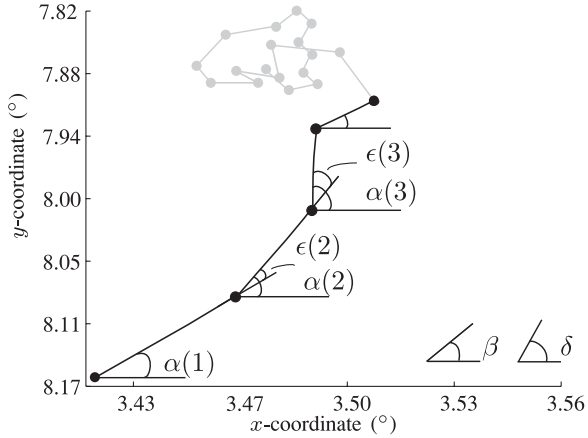

Fig. 5. An illustration of the calculation of the directions, $\alpha(n)$ and change in directions, $\epsilon(n), n = 1, 2, 3$, for the transition from a saccade (black) to a fixation (gray). In the lower right corner the thresholds, β for the change in sample-to-sample direction and δ for the deviation from the main direction are shown.

approximate saccadic intervals are together with the index vectors $I_x(n)$ and $I_y(n)$, shown in Fig. 4.

2) Saccadic Onset and Offset Detection: In the second part of the saccade detection, the exact onsets and offsets of the saccades are identified. For each approximate saccadic interval i the detection starts by determining the sample of maximum velocity, k_i. From sample k_i, the search for the exact onset and offset is performed using three criteria (a)–(c). These criteria are evaluated from sample k_i in the forward direction for the offset search, and in the backward direction for the onset search. In both directions, each criteria is compared to a predefined threshold. The exact onset and offset are set when at least one of the criteria is satisfied for a sufficient number of consecutive samples. The criteria are as follows.

a) *Deviation from the main direction.* Although a saccade often is slightly curved, an inherent physical property of saccades is that they do not deviate much from their main direction. In order to use this ballistic behavior to find the on- and offsets of the saccade, the sample-to-sample direction $\alpha(n)$ is employed. The sample-to-sample direction, $\alpha(n)$, is the angle to the x-axis of the vector between consecutive samples and is defined as

$$\alpha(n) = \arctan\left(\frac{d_y(n)}{d_x(n)}\right) \tag{1}$$

where $d_x(n)$ and $d_y(n)$ are the x- and y-components of the sample-to-sample velocity, respectively, i.e., $d_x(n) = x(n+1) - x(n)$ and $d_y(n) = y(n+1) - y(n)$. An illustration of the calculation of $\alpha(n)$ is shown in Fig. 5. The main direction γ is calculated as the average sample-to-sample direction of three consecutive samples centered around sample k_i, i.e., $\gamma = \frac{1}{3}(\alpha(k_i - 1) + \alpha(k_i) + \alpha(k_i + 1))$. In each direction, starting from sample k_i, the saccade begins/ends if $|\alpha(n) - \gamma| > \delta$ for $K = t_K \cdot F_s$ consecutive samples, where t_K is the threshold for the maximum duration of deviation from the main direction. Of the K samples exceeding the threshold, the onset/offset is set to the sample closest to k_i, see Fig. 6 for an example.

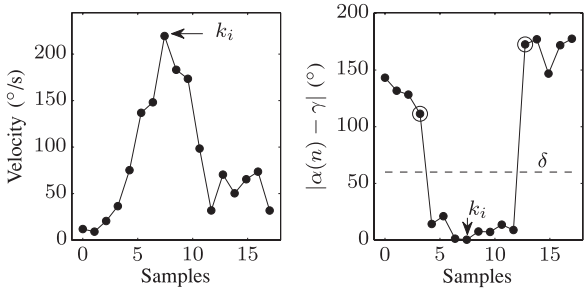

Fig. 6. An example of the principle for the on- and offset detection for criteria *a)*. Left: the velocity where k_i is marked. Right: deviation from the main direction, where the onset and offset are marked with (o), which in each direction is the sample closest to the k_i of the consecutive samples that have exceeded the threshold δ.

b) *Inconsistent sample-to-sample direction.* Due to the ballistic behavior of a saccade, it cannot abruptly change its direction from one sample to the next. The change in sample-to-sample direction $\epsilon(n)$ is calculated between consecutive samples in each approximate saccadic interval, and is defined as $\epsilon(n) = \alpha(n) - \alpha(n-1)$ (see Fig. 5). If the change in direction is larger than β,

$$|\epsilon(n)| > \beta \tag{2}$$

for $N = t_N \cdot F_s$ consecutive samples, where t_N is the threshold for the maximum duration of inconsistent sample-to-sample direction. The onset/offset is set to the sample most distant from k_i of the N samples that exceed the threshold.

c) *Distance between directional changes.* The distance between significant directional changes is measured as the Euclidean distance between samples satisfying $|\epsilon(n)| > \beta$. Thus, the number of such distances is lower than the number of samples. This third criterion exploits the fact that these distances are decaying when moving away from the center of the saccade and into the fixation. The onset and offset are reached when the eye is moving shorter

TABLE I
AN OVERVIEW OF THE PROPERTIES AND CRITERIA FOR THE DETECTION OF SACCADES AND PSO

Eye movement	Physiological property	Mathematical property	Criteria in the algorithm
saccade	fast movement	acceleration	acceleration threshold
		velocity	velocity threshold
saccade	ballistic	uniform direction	onset/offset criteria:
			(a) deviation from the main direction
			(b) inconsistent sample-to-sample direction
			(c) distance between directional changes
PSO	instability	decreasing oscillation	pole model and placement of the poles

distances before changing direction compared to the corresponding average distance in the intersaccadic intervals ν. In detail, when M consecutive distances are shorter than ν, the onset/offset is set to the position of the outermost such distance counted from sample k_i. The average distance between directional changes in the intersaccadic intervals ν is individually set for each recording and is calculated in a similar way as the distance between directional changes in the approximate saccadic intervals. However, the intersaccadic intervals may not only contain fixations, but also smooth pursuit movements. Therefore, a piecewise linear model of the signal is subtracted before the calculation of the average distance between directional changes. A block length of 100 ms was deemed sufficient for representation of the smooth pursuit movements while not interfering significantly to the calculation of ν. The residual positions $x'(n)$ and $y'(n)$ are used to calculate the residual direction $\alpha'(n)$ as

$$\alpha'(n) = \arctan\left(\frac{d'_y(n)}{d'_x(n)}\right) \tag{3}$$

where $d'_x(n)$ and $d'_y(n)$ are the x- and y-components of the residual velocity, respectively, i.e., $d'_x(n) = x'(n+1) - x'(n)$ and $d'_y(n) = y'(n+1) - y'(n)$. Next, the positions where the change in residual direction $\epsilon'(n)$ is larger than β is found,

$$|\epsilon'(n)| > \beta \tag{4}$$

where $\epsilon'(n) = \alpha'(n) - \alpha'(n-1)$ and the Euclidean distances between these positions are calculated. In order to robustly estimate ν, the value of the 90th percentile of these Euclidean distances is chosen.

In addition to criteria (b) and (c), the sample-to-sample velocity needs to be lower than 20% of the peak velocity for the current saccade to begin/end. The physiological motivations for the criteria used for saccade delineation are summarized in Table I.

C. PSO Detection

In the third part of the algorithm, the PSO are detected. PSO can physiologically be described as instabilities or oscillatory movements that may occur at the end of a saccade. The durations of PSO are in previous research shown to be between 10 to 35 ms [9]. In order to mathematically describe this property, an all-pole

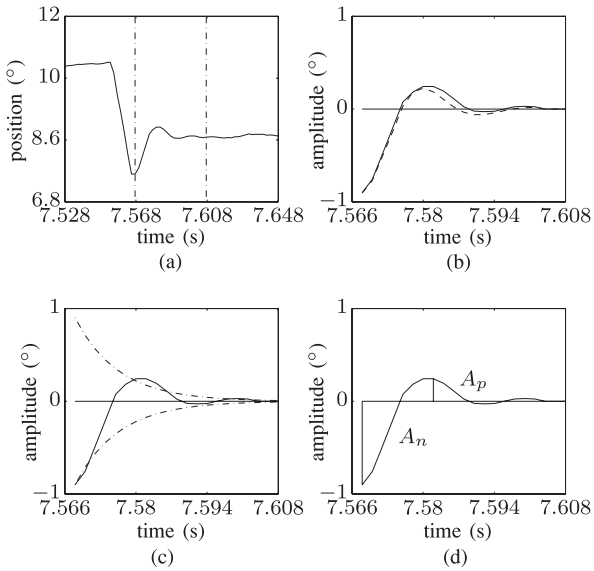

Fig. 7. An example of the principle for the detection of PSO. In (a) the interval used for the detection of PSO in the x-coordinate is shown. In (b), the interval is zoomed in and the signal $g(n)$ (solid) and its corresponding impulse response $\hat{g}_p(n)$ (dashed), with normalized RMSE = 0.07, are shown. In (c), the signal and its corresponding decaying component $f(n)$ and $-f(n)$ (dashed-dotted) are shown. In (d), the amplitudes A_p and A_n are shown together with $g(n)$.

model is employed. The model $g(n), n = 0, 1, \ldots, L-1$, where $L = t_L \cdot 10^{-3} F_s$ and F_s is the sampling frequency of the signal, is applied directly after the saccade offset. The x- and y-components of the interval are modeled separately, see Fig. 7(a) for an example of such interval. In order for the all-pole model to be meaningful, it is required that the signal is decaying. Therefore, in order to not include the beginning of a possible smooth pursuit movement in the signal to be modeled, a variable interval length L, corresponding to t_L ms, is considered. Initially t_L is set to 40 ms. If the oscillation is not ended before $t_L = 40$ ms, determined by different signs of the slopes fitted to the samples within 8 ms before and after the interval end, the initial interval length is extended to $t_L = 60$ ms. Starting from t_L, the interval is shortened in order to only include the entirety of the PSO by performing the following steps: a first-order polynomial is fitted from the end of $g(n)$ and to the left. In detail, one polynomial is fitted to $g(L-3)$ and $g(L-1)$; the slope of the polynomial is denoted as the reference slope. Another first-order polynomial is fitted to $g(L-4)$ and $g(L-3)$; this slope is denoted the test slope. The test slope is compared to the reference slope, and if the difference between the two slopes is less than θ the reference slope is extended one sample to the left, and the test slope is moved one sample to the left. The slopes are compared until the difference between them is larger than θ, indicating the beginning of a linear behavior in the end of $g(n)$. The entire reference slope interval is replaced by a constant level, corresponding to the level in the beginning of the replaced interval. In addition, in order for $g(n)$ to end at zero, $g(L-1)$ is subtracted from $g(n)$, as illustrated in Fig. 7(b). The following all-pole system function is employed,

$$G_p(z) = \frac{b_0}{1 + \sum_{k=1}^{p} a_p(k) z^{-p}} \tag{5}$$

where p is the order of the model, $a_p(k)$ are the coefficients of the model, and b_0 is a scaling factor. In order to estimate the coefficients $a_p(k)$ and the scaling factor b_0, Prony's method is used [22]. The correlation function $r_g(k)$ of $g(n)$ is calculated as

$$r_g(k) = \sum_{n=0}^{L-1} g(n)g(n-k). \tag{6}$$

By solving the following normal equations, the coefficients $a_p(k)$ are calculated

$$\sum_{l=1}^{p} a_p(l) r_g(k-l) = -r_g(k), \quad k = 1, \ldots, p. \tag{7}$$

In order to determine which order p of the model that best fits $g(n)$, the coefficients of the model are calculated for $p = 1, 2, 3, 4$. For each p, the root-mean-square error (RMSE) between $g(n)$ and the impulse response of the model, $\hat{g}_p(n)$, is calculated and normalized with the maximum absolute amplitude of the signal in the interval. The normalized RMSE for each order p is compared to the normalized RMSE for $p = 1$. If a higher order improves the normalized RMSE for $p = 1$ by 5% or more and the normalized RMSE is lower than 0.15, that order is used. If the normalized RMSE is larger than or equal to 0.15, the signal is shifted in time and the start of the modeling interval is iteratively moved one sample forward until the normalized RMSE is lower than 0.15. If none of the normalized RMSE satisfies this requirement, the model with the lowest normalized RMSE is employed. The poles of the polynomial for the selected order are calculated and for each pole the distance to the origin r indicates how quickly the signal decays to zero. A value of r close to zero indicates a fast decay while a value close to one indicates a slow decay. In order to summarize the distances from the poles to origin for models with $p > 1$, the maximum value $r_{\max}$ is used. In order for the signal to be identified as PSO, $\hat{g}_p(n)$ must have $r_{\max} < r_{\text{th}}$ and a maximum absolute amplitude $A > A_{\min}$. The offsets of the PSO are determined by using the function $f(n) = Ar_{\max}^n$, which describes the decaying component of the modeled signal (see Fig. 7(c)). The difference between $\hat{g}_p(n)$ and $f(n)$ is calculated as

$$u(n) = \begin{cases} \hat{g}_p(n) - f(n), & \text{if } \sum \hat{g}_p(n) < 0 \\ \hat{g}_p(n) - (-f(n)), & \text{if } \sum \hat{g}_p(n) > 0. \end{cases}$$

The offsets of the PSO are defined as the first sample where $u(n) < \xi$ during $R = t_R \cdot F_s$ consecutive samples. In order to not detect very slow movements, the following ratio between the amplitude and the duration of the PSO are calculated:

$$s = \frac{A_n + A_p}{t_g} \tag{8}$$

where A_n is the maximum absolute amplitude of the negative part of $g(n)$, A_p is the maximum amplitude of the positive part of $g(n)$, and t_g is the duration of the detected PSO (see Fig. 7(d)). All PSO that have $s < \frac{0.4 \cdot 10^3}{2F_s}$ are discarded. If PSO are detected in both the x- and y-components, the offset is set to the index that corresponds to the latest offset.

D. Performance Evaluation

In order to evaluate the performance of the algorithm in terms of sensitivity and specificity, (cf., [23]), a manually annotated database is used as a reference. The sensitivity describes the algorithms ability to correctly classify each type of eye movement and a value close to one is desired. For each type of eye movement i, where $i = \{S = \text{Saccade}, \text{PSO} = \text{Postsaccadic oscillations}, D = \text{Disturbances}, SF = \text{Smooth pursuit/Fixation}\}$, the sensitivity_i is calculated as

$$\text{sensitivity}_i = \frac{\text{TP}_i}{\text{TP}_i + \text{FN}_i} \tag{9}$$

where $true\ positives$ TP_i is the number of correctly classified samples for eye movement type i, and the $false\ negatives$ FN_i is the number of samples that the algorithm falsely classified as eye movement type i.

The specificity_i describes the algorithms ability to only find the samples of eye movement type i and a value close to one is desired. For each type of eye movement i, the specificity_i was calculated as

$$\text{specificity}_i = \frac{\text{TN}_i}{\text{TN}_i + \text{FP}_i} \tag{10}$$

where $true\ negatives$ TN_i is the number of samples that the algorithm correctly classified as another type of eye movement than i. The $false\ positives$ FP_i is the number of samples that should have been classified as eye movement type i, but have incorrectly been classified as another type of eye movement.

The comparison between the manual annotation and the detections of the algorithm is summarized by Cohen's kappa [24] κ,

$$\kappa = \frac{P_o - P_e}{1 - P_e}, \quad \kappa \in [0, 1] \tag{11}$$

where P_o is the observed proportion of agreement between the output of the algorithm and the manual annotation, and P_e is the proportion of agreement expected by chance between the output of the algorithm and the manual annotation. For a detailed description on the calculation of P_o and P_e, see [25]. A value of κ close to one is desired, and indicates that there is an overall good agreement between the algorithm and the manual annotation.

The proposed algorithm is also compared to the adaptive velocity-based algorithm described in [9]. This algorithm was chosen because it is one of few algorithms that is able to detect PSO and is freely available. In addition, it outperformed two of the most commonly used algorithms today: the identification by velocity threshold (I-VT) algorithm and the identification by dispersion threshold (I-DT) algorithm [9]. In order to be able to compare different algorithms which may detect different numbers and lengths of each type of eye movement, the entire performance evaluation is based on the classification of each sample.

III. Experiment and Database

The eye-tracking signals used in this paper were collected in an experiment where 33 participants, students, and personnel from Lund University took part. The mean age of the

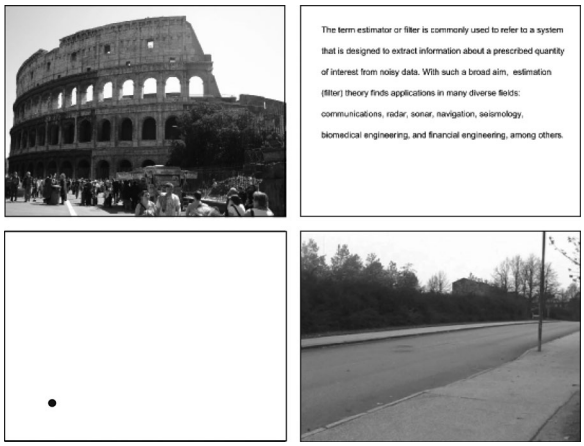

Fig. 8. An example of the different types of stimuli used in the experiment. Upper left: Image, upper right: Text, lower left: moving dot and lower right: a frame of a video clip.

TABLE II
A SUMMARY OF THE EXPERIMENT

Blocks	Content	Annotated/Total
Image	**photographs with nature motives**	14/155
Text	texts	-
Moving dot	**one black dot on white background** in 8 directions $(0, \pm\frac{\pi}{4}, \pm\frac{\pi}{2}, \pm\frac{3\pi}{4}, \pi)$ 4 speeds (**5**, 10, **20**, 30°/s)	11/62
	sinusoid	-
	blinking static dots	-
Video clip	**real-world videos with moving objects,** e.g, road with traffic and a roller coaster	9/186
Scrolling text	vertical scrolling text	-

In this paper the stimuli marked in bold font are used.

participants was 31.2 ± 9.9 (M $\pm$ SD) years. In the experiment, two computers were used, one for showing the stimuli and one for controlling the eye-tracker. Stimuli were presented using MATLAB R2009b and Psychophysics toolbox (version 3.0.8, Revision 1591), on a Samsung Syncmaster 931c TFT LCD 19 inch (380 mm$\times$300 mm) monitor, with a screen refresh rate of 60 Hz and a resolution of 1024$\times$768 pixels. The computer controlling the eye-tracker was running iView X (version 2.4.19). The signals were recorded binocularly with the iView X Hi-Speed 1250 eye-tracker from SensoMotoric Instruments (Berlin, Germany), at a sampling frequency of 500 Hz. The viewing distance from the eye-tracker to the screen was 670 mm. At the start of the experiment, a calibration procedure was performed for each participant. The calibration procedure contained a nine-target binocular calibration in iViewX followed by four targets used to validate the accuracy of the calibration. The average accuracy across participants and validation targets was 0.41° and 0.41° for the x- and y-components, respectively.

The experiment contained five blocks with different types of stimuli: images, texts, moving dots, short video clips, and a scrolling text. Examples of the stimuli are shown in Fig. 8, and a summary of the content in the different blocks is shown in Table II. Each block contained a number of trials with the same type of stimuli. Both the block order and the internal trial order within the block were randomized for each participant. Before the next trial started, the participants were instructed to fixate at a centrally located cross. Before a new block started, the participants were given detailed written instructions on the screen about the next task. These instructions were: to freely view an image for 10 s, to read a text at your own speed, and to follow moving dots and moving objects for video clips.

The database used in this paper is a subset of the complete database recorded during the described experiment. From now on, in this paper, the database refers to the signals recorded from participants viewing images, moving dots, and video clips. These trials are marked with bold font in Table II. Of the 33 participants that were included in the experiment, 31 were used; two participants were excluded due to saving problems during the recording process. Only signals recorded from the right eye were used in the analysis. The database was divided into two parts by splitting the participants into two equally large groups; one part for development and one part for the testing of the algorithm.

A subset of the signals from both the development part and the test part of the database was annotated manually by a domain expert (author MN[1]). In order to facilitate the annotation process, a GUI was developed in MATLAB, showing the x- and y-coordinates over time, the velocity over time, the vertical diameter of the pupil over time, the coordinates in the xy-space, and a zoomed in version of the last manually annotated event in the xy-space. These representations were judged sufficient for the expert to reliably detect the eye movements. The expert classified each sample into six different types of events: fixations, saccades, PSO, smooth pursuit movements, blinks, and undefined events. An undefined event is when a sample does not conform to any of the other eye movements. The manual annotation was performed without knowing beforehand which type of stimulus that was used. In order to ensure that a representative set of signals were used both for the development and for the evaluation of the algorithm, the manual annotation set was chosen with respect to the quality of the signals; half of the selected signals for each type of stimuli had a lower quality and the other half had a higher quality. In order to determine the quality of the signals, the percentage of data loss and the average distance between directional changes in the intersaccadic intervals ν were computed. The term data loss contained both the amount of blinks and the amount of samples with unreasonable high velocities and accelerations. The blink detection described in the preprocessing part was used. A signal was judged to have a high quality when both the amount of data loss and ν were lower than respective median of the two measures and the opposite was true for signals exhibiting lower qualities.

IV. RESULTS

The settings of all intrinsic algorithm parameters, given in Table III, were used in the entire results section. All intrinsic parameters were adjusted using only the development part of the

[1]Examples of the manually annotated part of the database can be downloaded as a pdf at www.eit.lth.se/staff/linnea.larsson

TABLE III
THE SETTINGS FOR THE INTRINSIC PARAMETERS IN THE PROPOSED ALGORITHM FOR ALL TYPES OF STIMULI

Parameter	Value	Description
Preprocessing		
$a_{\min}$	0.3°	Min. amplitude for a one-sample spike
Saccade detection		
$t_{\min}$	20 ms	Min. time between two saccades
T	6 ms	Min. duration of a saccade
λ	6	No. standard deviations for η_x and η_y
δ	60°	Max. allowable deviation from the main direction
t_K	6 ms	Max. duration of deviation from the main direction
β	40°	Largest allowable change in intra-saccadic direction
t_N	8 ms	Max. duration of inconsistent sample-to-sample direction
M	2	No. distances below ν
θ	1.7	Min. difference between ref. slope and test slope
PSO detection		
r_{th}	$0.89^{500/F_s}$	Max. distance from origin to a pole
t_L	40 ms	Initial length of the interval for PSO modeling
$A_{\min}$	0.2°	Min. amplitude for PSO
ξ	0.08°	Min. value of the difference between the decaying component and the modeled signal
t_R	6 ms	Max. duration of ξ

Note that the ° notation in the cases of δ and β refers to an angle in the image plane on the stimulus screen while it in all other cases represent degrees of visual angle.

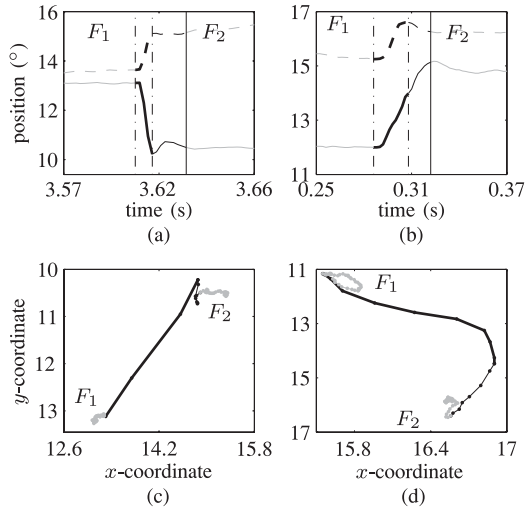

Fig. 9. Two examples of the detection of saccades and PSO, where (a)–(b) are showing the x- and y-components over time and (c)–(d) are showing the xy-domain for the two examples. The thicker black line marks the saccades, the thinner black line the PSO, the vertical dash-dotted line the on- and offsets of the saccades, the solid vertical black line the offsets of the PSO and the gray line corresponds to the fixations, F_1 and F_2, before and after the saccade in each case.

database. Two examples of the detection of saccades and PSO for two different types of PSO recorded during image stimuli are shown in Fig. 9, in both the time and the xy-domain.

A. Evaluation of the Algorithm

In order to evaluate the performance of the proposed algorithm, the eye movements detected by the algorithm are compared to the manually annotated eye movements and to those detected by the velocity-based adaptive algorithm described in [9]. Six properties of the detected saccades and PSO are presented in Table IV, for the annotated part of the database. For comparison, the corresponding values for the entire development part of the database are shown in brackets. The durations of the saccades detected by the proposed algorithm are in agreement with the durations of those detected by the expert, while the saccades detected by the algorithm in [9] are in general longer, 40–50 ms compared to 23–29 ms for the expert. The issue with longer durations of the detected saccades is mentioned in [9]. The durations of the PSO detected by the proposed algorithm are in general slightly longer than those detected by the expert and the durations of the PSO detected by the algorithm in [9] are longer than those detected by both the expert and the proposed algorithm. Around 85% of all saccades detected by the expert have PSO for image and video stimuli. For moving dot stimuli, the expert detects 65% saccades with PSO. The proposed algorithm detects close to equally many PSO as the expert. The algorithm in [9] detects a lower number of saccades and in addition also fewer PSO for all types of stimuli compared to the expert.

The sensitivities and specificities for the detection of saccades, PSO, disturbances, and periods of smooth pursuit movements and/or fixations are shown in Table V. Disturbances include everything that is not detected as eye movements, i.e., blinks, screen outliers, and one-sample spikes. The eye movements included in the category of smooth pursuit movements and/or fixations correspond to samples that the algorithm does not count as saccades, PSO, or disturbances. The performance of the saccade detection for the two algorithms is equally good with specificity above 0.93 and sensitivity above 0.80, for all stimuli. However, it should be noted in Table IV that the durations of the saccades differ between the two algorithms and the similarities in sensitivities and specificities are due to that the proposed algorithm detects a larger and more correct number of saccades with shorter durations in contrast to the algorithm in [9] that detects a lower number of saccades with longer durations.

For the detection of PSO, there is a larger difference between the two compared algorithms, where the proposed algorithm outperforms the algorithm in [9]. The values of the sensitivity are 0.73–0.76 for the proposed algorithm compared to 0.14–0.37 for the algorithm in [9]. Both algorithms have equally high specificities, with values in the range of 0.96–0.99. The lower level of the sensitivity for the two algorithms indicates that there are too few samples that are detected as PSO compared to the annotation. Since the two algorithms have different strategies for the detection of disturbances, the sensitivities and specificities for the two algorithms differ. The proposed algorithm detects the disturbances with high specificity, 0.99, and a slightly lower sensitivity, 0.67–0.89, than the algorithm in [9], with specificity 0.67–0.85 and sensitivity 0.97–1. The algorithm in [9] puts in general more uncertain samples in the disturbance category. These different strategies for the detection of disturbances also affect those samples that become marked as smooth pursuit movements and/or fixations.

In order to summarize the general performance of the two detection algorithms for all types of eye movements, Cohen's kappa κ which measures the interobserver agreement, is computed as described in Section II-D. The κ for the two algorithms summarized for all types of stimuli are shown in Table VI. In general, κ for the proposed algorithm is considerably larger than κ for the algorithm in [9]. In order to validate the results from the development part of the database, κ was also computed for

TABLE IV
MEAN VALUES FOR THE PROPERTIES OF THE DETECTED SACCADES AND PSO FOR THE EXPERT (EXP), THE PROPOSED ALGORITHM (PROP.), AND THE ALGORITHM DESCRIBED IN [9]

	Image					Video					Moving dot				
Measure	Exp	Prop.		Alg. [9]		Exp	Prop.		Alg. [9]		Exp	Prop.		Alg. [9]	
Saccade duration (ms)	28.7	28.1	(29)	50	(49.1)	23.9	26.6	(26.4)	40.2	(43.1)	23.5	25	(28.2)	43.4	(43.5)
Saccade peak velocity (°/s)	404	394	(316)	383	(327)	335	316	(281)	321	(299)	265	163	(200)	174	(206)
PSO duration (ms)	20.4	24.6	(25.8)	25.8	(23.7)	21.2	23.4	(24.9)	24	(23.7)	14.7	20.6	(23.8)	24	(22.8)
% of saccades with PSO	84.5	83.9	(77.4)	69.2	(62.7)	85.7	78.7	(74.2)	82.9	(61.1)	62.1	54.5	(66)	41.7	(39.1)
Number detected saccades	283	286	(2310)	266	(2073)	84	89	(7231)	76	(6016)	29	33	(106)	24	(87)
Number detected PSO	239	240	(1789)	184	(1300)	72	70	(5362)	63	(3675)	18	18	(70)	10	(34)

In brackets, the corresponding value for the entire development part of the database is shown.

TABLE V
SENSITIVITY AND SPECIFICITY FOR THE PROPOSED ALGORITHM (PROP.) AND THE ALGORITHM IN [9]

	Image		Video		Moving dot	
	Prop.	Alg. [9]	Prop.	Alg. [9]	Prop.	Alg. [9]
Sensitivity_S	0.838	0.907	0.893	0.89	0.815	0.801
Specificity_S	0.984	0.926	0.983	0.963	0.982	0.968
Sensitivity_{PSO}	0.758	0.244	0.753	0.369	0.727	0.144
Specificity_{PSO}	0.973	0.957	0.986	0.973	0.989	0.987
Sensitivity_D	0.882	0.965	0.892	1	0.667	1
Specificity_D	0.992	0.846	0.999	0.809	0.999	0.665
Sensitivity_{SF}	0.955	0.739	0.973	0.751	0.978	0.614
Specificity_{SF}	0.885	0.978	0.895	0.971	0.828	0.949

TABLE VI
COHENS KAPPA FOR THE PROPOSED ALGORITHM AND THE ALGORITHM IN [9] FOR THE DEVELOPMENT PART OF THE DATABASE

	Image	Video	Moving dot
Proposed algorithm	0.814	0.822	0.756
Algorithm in [9]	0.512	0.398	0.232

TABLE VII
COHENS KAPPA FOR THE PROPOSED ALGORITHM AND THE ALGORITHM IN [9] FOR THE TEST PART OF THE DATABASE

	Image	Video	Moving dot
Proposed algorithm	0.745	0.804	0.736
Algorithm in [9]	0.484	0.336	0.288

TABLE VIII
PERCENTAGE (%) OF USE FOR EACH CRITERION IN THE SACCADE ON- AND OFFSET DETECTION

	Image	Video	Moving dot
Saccade onset			
(a) Deviation from the main direction	75.3	76.3	69.9
(b) Inconsistent sample-to-sample direction	21.3	19	24.3
(c) Distance between directional changes	3.25	4.78	5.65
Saccade offset			
(a) Deviation from the main direction	63.4	67.2	66
(b) Inconsistent sample-to-sample direction	23.8	16.7	15.1
(c) Distance between directional changes	12.8	16.2	18.9

the test part of the database, see Table VII. The results for the test part of the database are comparable with the results for the development part of the database.

B. Evaluation of Parameter Settings

The parameter settings shown in Table III are chosen according to known physiological limitations of eye movements, visual inspection of detection results using the development part of the database, and the previous literature. Table VIII shows how often the criteria (a)–(c) are employed in the detection of the saccadic on- and offsets. As shown in Table VIII, all the suggested criteria are used for the detection of both on- and offsets of the saccades. The criterion deviation from the main direction is the most commonly used criterion, (63–76%), for the detection of both on- and offsets. The least used criterion is the distance between directional changes.

V. DISCUSSION

An algorithm for the detection of saccades and PSO in eye-tracking signals was proposed. The proposed algorithm has been tested on signals recorded during both static and dynamic stimuli, where the latter contained smooth pursuit movements. Its performance was evaluated in comparison to manually annotated eye movements and an adaptive velocity-based algorithm, described in [9].

The performance of the saccade detection was in terms of sensitivity and specificity generally similar to the algorithm in [9]. However, the durations and the number of saccades differed between the two algorithms. The lower number of saccades using the algorithm in [9] can be explained by the presence of smooth pursuit movements in the signal, which increases the velocity threshold such that small saccades are missed. The reason for the longer durations for the algorithm in [9] is that it solely uses a velocity threshold, and searches for a local minima in the velocity before and after the peak, while the proposed algorithm uses a combination of several criteria, for the detection of the on- and offsets of the saccades.

The appearance of PSO is highly dependent on the type of eye-tracker that is used [16], and PSO have therefore been treated unsystematically, or not at all by most algorithms. Explicitly detecting and modeling of PSO, as is described in this paper, leaves the user with several options: the PSO can be: 1) included in the saccades, 2) included in the subsequent eye movements, 3) classified as its own type of eye movement, 4) discarded because of its unknown perceptual and cognitive consequences, or 5) substituted by a simplified first order all-pole model in order to suppress the PSO. Different options may be suitable for different types of research and are all supported by the proposed method.

There was a large difference in the performance of the detection of PSO between the two compared algorithms. The two algorithms use two completely different strategies for the detection of the PSO, where the proposed algorithm uses an all-pole model, while the algorithm in [9] uses an adaptive velocity threshold. By using a model, the proposed algorithm was, in

addition to perform more accurate offsets detection of the PSO, also able to identify different types of PSO that was not possible when only using the velocity signal. According to the properties of the detected PSO in Table IV, there appears to be no difference in duration between PSO measured during image and video stimuli in this database.

The quality of the signals used for the evaluation of the proposed algorithm has been measured. Signals with both higher and lower quality have been used both for the development and testing of the algorithm. It has, however, not been evaluated if there is a difference in performance for signals with different level of quality.

The algorithm was also tested for the same database downsampled to 250 Hz with a similar/slightly degraded performance (Cohens kappa = 0.78, 0.76, and 0.70 for image, video, and moving dot stimuli) and for text reading data (ten cases of in total 395 s) sampled at 1250 Hz where the performance was in good agreement with the performance when running the same data downsampled to 500 Hz (Cohens kappa = 0.80).

The proposed algorithm is intended for offline use. Since the velocity filter is not causal and the proposed algorithm performs segmentation of the signals before the final classification, it is not suitable for real-time applications.

The eye movements detected by the proposed algorithm are compared to manual annotation performed by an expert. By using the annotated eye movements, the performance of the algorithm was quantitatively evaluated. Since the annotation is performed on a sample-to-sample basis, the exact performance of the detection algorithm can be evaluated in contrast to previously used evaluation methods where, e.g., statistics of amplitudes, durations, or number of detected events have been calculated and evaluated [9], [12]. By using a combination of the measures and values in Tables IV–VI, the performance of the algorithm can be evaluated at different scales, from the exact on- and offsets of individual events to Cohen's kappa which summarizes all sensitivities and specificities over the entire annotated part of the database.

VI. Conclusion

In this paper, an algorithm for the event detection and eye movement classification based on eye-tracking signals is proposed. In summary, the proposed algorithm provides more accurate on- and offsets estimation of the saccades, outperforms a previously suggested estimation method for PSO, and in addition allows modeling of the PSO. Furthermore, a methodological framework for the objective testing of event detection algorithms applied to eye-tracking signals have been developed, including a large partly annotated, database recorded during both static and dynamic stimuli, a GUI for easy annotation and viewing of eye movement events, and an evaluation procedure which summarizes the overall performance into one Cohen's kappa value.

References

[1] T. Crawford, S. Higham, T. Renvoize, J. Patel, M. Dale, A. Suriya, and S. Tetley, "Inhibitory control of saccadic eye movements and cognitive impairment in alzheimer's disease," *Biol. Psychiatry*, vol. 57, pp. 1052–1060, 2005.

[2] J. Sweeney, B. Brew, J. Keilp, J. Sidtis, and R. Price, "Pursuit eye movement dysfunction in HIV-1 seropositive individuals," *J. Psychiatry Neurosci.*, vol. 16, no. 5, pp. 247–252, 1991.

[3] K.-M. Flechtner, B. Steinacher, R. Sauer, and A. Mackert, "Smooth pursuit eye movements in schizophrenia and affective disorder," *Psychol. Med.*, vol. 27, pp. 1411–1419, 1997.

[4] K. Holmqvist, M. Nyström, R. Andersson, R. Dewhurst, H. Jarodzka, and J. van de Weijer, *Eye Tracking: A Comprehensive Guide to Methods and Measures*. Oxford, U.K.: Oxford Univ. Press, 2011.

[5] R. Leigh and D. Zee, *The Neurology of Eye Movements*. Oxford, U.K.: Oxford Univ. Press, 2006.

[6] C. Meyer, A. Lasker, and D. Robinson, "The upper limit of human smooth pursuit," *Vis. Res.*, vol. 25, no. 4, pp. 561–563, 1985.

[7] A. T. Bahill, M. R. Clark, and L. Stark, "Glissades-eye movements generated by mismatched components of the saccadic motoneuronal control signal," *Math. Biosci.*, vol. 26, pp. 303–318, 1975.

[8] D. Salvucci and J. Goldberg, "Identifying fixations and saccades in eye-tracking protocols," in *Proc. Symp. Eye Tracking Res. Appl.*, 2000, pp. 71–78.

[9] M. Nyström and K. Holmqvist, "An adaptive algorithm for fixation, saccade, and glissade detection in eyetracking data," *Behav. Res. Methods*, vol. 42, no. 1, pp. 188–204, 2010.

[10] R. Engbert and R. Kliegl, "Microsaccades uncover the orientation of covert attention," *Vis. Res.*, vol. 43, no. 9, pp. 1035–1045, 2003.

[11] F. Behrens, M. MacKeben, and W. Schröder-Preikschat, "An improved algorithm for automatic detection of saccades in eye movement data and for calculating saccade parameters," *Behav. Res. Methods*, vol. 42, no. 3, pp. 701–708, 2010.

[12] R. van der Lans, M. Wedel, and R. Pieters, "Defining eye-fixation sequence across individuals and tasks: The binocular-individual threshold (bit) algorithm," *Behav. Res. Methods*, vol. 43, no. 1, pp. 239–257, 2011.

[13] P. Mital, T. Smith, R. Hill, and J. Henderson, "Clustering of gaze during dynamic scene viewing is predicted by motion," *Cognitive Comput.*, vol. 3, no. 1, pp. 5–24, 2010.

[14] M. Dorr, T. Martinez, K. Gegenfurtner, and E. Barth, "Variability of eye movements when viewing dynamic natural scenes," *J. Vision*, vol. 10, no. 28, pp. 1–17, 2010.

[15] SR Research Ltd. *EyeLink User Manual*. Kanata, Ontario, Canada. Version 1.3.0, 2007.

[16] H. Deubel and B. Bridgeman, "Fourth Purkinje image signals reveal eye-lens deviations and retinal image distortions during saccades," *Vis. Res.*, vol. 35, no. 4, pp. 529–538, 1995.

[17] M. Bettenbühl, C. Paladini, M. Holschneider, K. Mergenthaler, R. Kliegl, and R. Engbert, "Microsaccade characterization using the continuous wavelet transform and principal component analysis," *J. Eye Movement Res.*, vol. 3, no. 5, pp. 1–14, 2010.

[18] O. Komogortsev, D. Gobert, S. Jayarathna, D. Hyong Koh, and S. Gowda, "Standardization of automated analyses of oculomotor fixation and saccadic behaviors," *IEEE Trans. Biomed. Eng.*, vol. 57, no. 11, pp. 2635–2645, Nov. 2010.

[19] Z. Kapoula, D. Robinson, and T. Hain, "Motion of the eye immediately after a saccade," *Exp. Brain Res.*, vol. 61, no. 2, pp. 386–394, 1986.

[20] D. Stampe, "Heuristic filtering and reliable calibration methods for video-based pupil tracking systems," *Behav. Res. Methods Instrum. Comput.*, vol. 25, no. 2, pp. 137–142, 1993.

[21] J. Otero-Millan, X. Troncoso, S. Macknik, I. Serrano-Pedraza, and S. Martinez-Conde, "Saccades and microsaccades during visual fixation, exploration, and search: Foundations for a common saccadic generator," *J. Vision*, vol. 8, no. 14, pp. 1–18, 2008.

[22] M. Hayes, *Statistical Digital Signal Processing and Modeling*. New York, NY, USA: Wiley, 1996.

[23] L. Sörnmo and P. Laguna, *Bioelectrical Signal Processing in Cardiac and Neurological Applications*. New York, NY, USA: Elsevier, 2005.

[24] C. Jean, "Assessing agreement on classification tasks: The kappa statistic," *Comput. Linguistics*, vol. 22, no. 2, pp. 249–254, 1996.

[25] K. Berry and P. Mielke, "A generalization of Cohen's kappa agreement measure to interval measurement and multiple raters," *Edu. Psychol. Meas.*, vol. 48, pp. 921–933, 1988.

Authors' photographs and biographies not available at the time of publication.